Radio Science, Volume 18, Number 2, pages 175–186, March–April 1983

Real axis integration of Sommerfeld integrals: Source and observation points in air

W. A. Johnson

Electronics Engineering Department, Lawrence Livermore National Laboratory, Livermore, California 94550

D. G. Dudley

Department of Electrical Engineering, University of Arizona, Tucson, Arizona 85721

(Received April 16, 1982; revised September 27, 1982; accepted September 27, 1982.)

Change of variables and subtraction of asymptotic terms are used to aid in the integration of Sommerfeld integrands along the real axis. The change of variables smooths oscillations which would otherwise become densely packed at the associated branch point. Subtraction of asymptotic terms is used to speed up the truncation process of an otherwise infinite integration interval. Interest is restricted to practical earth parameters and frequencies above 2 MHz. Comparison with a complex contour technique shows the present method to be particularly well suited for the analysis of a vertical, thin-wire antenna in the presence of a lossy earth.

1. INTRODUCTION

Conventional techniques for the analysis of scattering and radiation by antennas in the presence of a lossy earth require numerous evaluations of Sommerfeld integrals. With this motive to obtain efficient, accurate methods of evaluating Sommerfeld integrals, a vast literature has been produced [*Rahmat-Samii et al.*, 1981].

Direct numerical integration techniques have the advantage of a wide range of validity in medium, frequency, and spatial parameters. The major limitation of these techniques is computation time.

Siegel and King [1970] numerically integrated Sommerfeld integrands along the real axis. Their technique is applicable to both vertical and horizontal dipoles with arbitrary source and observation point locations. To avoid difficulties associated with integrating highly oscillatory integrands, Romberg integration was performed between the zeros of Bessel functions which occur in the Sommerfeld integrands. Modifications of the Romberg scheme were made to integrate carefully over regions where the integrand becomes singular. To accelerate the process of truncating the infinite integration interval, a Euler summation method was used. *Bubenik* [1977] improved this truncation process by use of Shank's summation technique, when he evaluated the magnetic field due to a quasi-static vertical electric dipole.

Integration along contours in the complex plane has been used to avoid singularities and reduce oscillations of the integrand. *Burke et al.* [1981] used Romberg-Shanks integration along complex contours to compute electric fields of vertical and horizontal electric dipoles when both source and observation points were located above a lossy ground. *Parhami et al.* [1980] evaluated Sommerfeld integrals, associated with the vector potential of a horizontal dipole with source and observer in air, by integrating along the steepest descent path with a Gauss-Laguerre quadrature.

To avoid integration along complex contours and the associated effort of computing Bessel functions with complex arguments, we use analytical techniques to remove singularities and reduce oscillations that occur when Sommerfeld integrands are evaluated along the real axis. The computation of electric fields due to vertical and horizontal electric dipoles is considered. For brevity, source and observation points are restricted to lie in air. Figure 1 illustrates the problem geometries for both vertical and horizontal electric dipoles. Of course, limitations on com-

Paper number 2S1545.

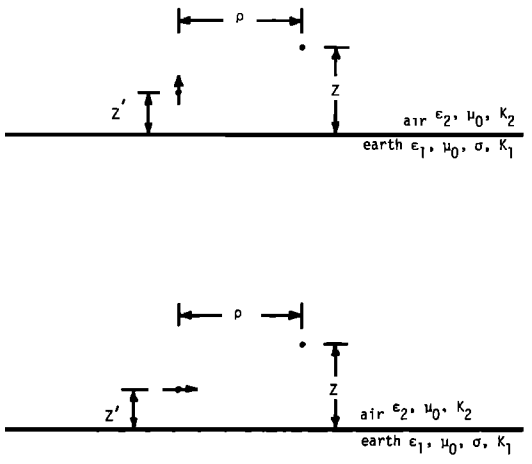

Fig. 1. Problem geometries for vertical and horizontal electric dipoles. The air parameters are an electric permittivity ε_2, a magnetic permeability μ_0, and a wave number K_2. The ground has a permittivity ε_1, a permeability μ_0, a conductivity σ, and a complex wave number K_1.

puter time will restrict the distances $z + z'$ and ρ (Figure 1) from becoming too large in terms of the free-space wavelength.

The present integration technique will use local change of variables to remove singularities, as well as rapidly varying oscillations, that occur along the real axis in the vicinity of a branch point. A compound Simpson's rule [*Davis and Rabinowitz*, 1975] is chosen to integrate over half-cycles of the integrand's oscillations. Subtraction of asymptotic terms, a technique with similarities to the work of *Rana and Alexopoulos* [1981], is used when necessary to speed up the process of truncating the infinite integration interval. Although our particular interest is in practical earth parameters, i.e., a dielectric constant less than 16 and a conductivity less than 0.01 mhos per meter, the technique is valid over a wider range of parameters. The major limitation of the technique is that when the magnitude of K_1^2/K_2^2 is larger than 90, subtraction of asymptotic terms becomes inefficient. The change of variable technique remains applicable for ratios of K_1^2/K_2^2 with magnitude larger than 600,000. Graphical illustrations show the effects of both the change of variables and subtraction of asymptotic terms for typical integrands. Comparison of results shows the present real axis integration technique has definite advantage over the complex contour methods of *Burke et al.* [1981] when the radial separation ρ between source and observation point is small with respect to the sum of the source and observation heights $z + z'$.

2. FORMULATION

The electric field of vertical and horizontal electric dipoles with source and observation points in air may be expressed as the sum of free-space and image Green's functions plus 5 Sommerfeld integrals [*Banos*, 1966]. These integrals are $((\partial^2/\partial z^2) + K_2^2)V_{22}$, U_{22}, $(\partial^2/\partial\rho\,\partial z)V_{22}$, $(-\partial/\partial\rho)V_{22}$, and $(\partial^2/\partial\rho^2)V_{22}$, where

$$U_{22} = 2\int_0^\infty \frac{e^{-\gamma_2|z+z'|}}{\gamma_1+\gamma_2}\,\lambda J_0(\lambda\rho)\,d\lambda \tag{1}$$

$$V_{22} = 2\int_0^\infty \frac{e^{-\gamma_2|z+z'|}}{K_2^2\gamma_1 + K_1^2\gamma_2}\,\lambda J_0(\lambda\rho)\,d\lambda \tag{2}$$

$$K_i = \omega\left[\mu_0\left(\varepsilon_i - \frac{j\sigma_i}{\omega}\right)\right]^{1/2}$$

$$\mathrm{Re}\,(K_i) > 0 \qquad \mathrm{Im}\,(K_i) \le 0 \qquad i = 1, 2 \tag{3}$$

and

$$\gamma_i = (\lambda^2 - K_i^2)^{1/2}$$

$$\mathrm{Re}\,(\gamma_i) \ge 0 \qquad \mathrm{Im}\,(\gamma_i) \le 0 \qquad i = 1, 2 \tag{4}$$

Since

$$\frac{\partial^2}{\partial\rho^2}V_{22} = -\frac{1}{\rho}\frac{\partial}{\partial\rho}V_{22} - \left(\frac{\partial^2}{\partial z^2} + K_2^2\right)V_{22} \tag{5}$$

it is sufficient to consider the numerical evaluation of the first 4 Sommerfeld integrals. It is convenient to express these quantities as

$$\begin{bmatrix} \left(\dfrac{\partial^2}{\partial z^2} + K_2^2\right)V_{22} \\ U_{22} \\ \dfrac{\partial^2}{\partial\rho\,\partial z}V_{22} \\ -\dfrac{\partial}{\partial\rho}V_{22} \end{bmatrix} = 2\int_0^\infty \bar{I}(\lambda, |z+z'|, \rho)\,d\lambda \tag{6}$$

with

$$\bar{I}(\lambda, w, \rho) = \begin{bmatrix} I1 \\ I2 \\ I3 \\ I4 \end{bmatrix} = e^{-\gamma_2 w}\begin{bmatrix} \dfrac{\lambda^3}{K_1^2\gamma_2 + K_2^2\gamma_1}J_0(\lambda\rho) \\ \dfrac{\lambda}{\gamma_2+\gamma_1}J_0(\lambda\rho) \\ \dfrac{\gamma_2\lambda^2}{K_1^2\gamma_2 + K_2^2\gamma_1}J_1(\lambda\rho) \\ \dfrac{\lambda^2}{K_1^2\gamma_2 + K_2^2\gamma_1}J_1(\lambda\rho) \end{bmatrix} \tag{7}$$

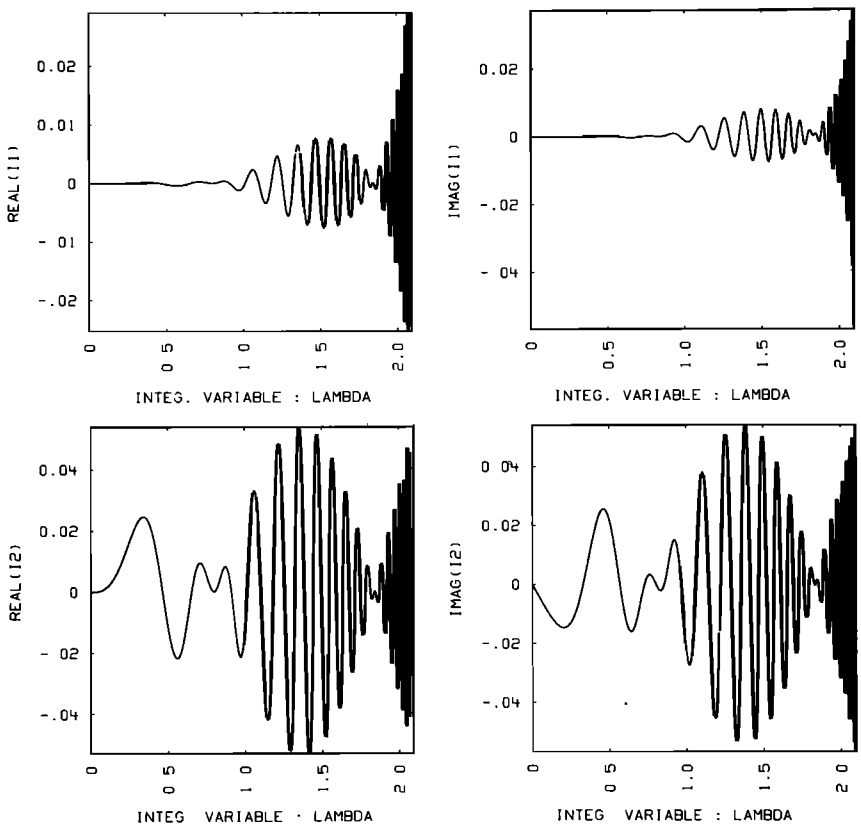

Fig. 2. Integrand behavior in the λ interval $[0, K_2]$. Parameters: $f = 10^8$ Hz, $\varepsilon_r = 16$, $\sigma = 10^{-4}$ mhos/m, $\rho = 1\lambda_0$, and $z + z' = 20\lambda_0$.

and $\gamma_i (i = 1, 2)$ given by (44). It is noted that if $|z + z'|$ is set to zero in (6), the integral becomes undefined. This problem will be remedied in the next section.

3. NUMERICAL CONSIDERATIONS

Obstacles to efficient evaluation of the Sommerfeld integrals (equations (6) and (7)) are now considered. A means of overcoming each obstacle is presented, and a brief description of a numerical integration procedure is given. Graphical results are chosen to illustrate typical integrand behavior before and after each obstacle has been overcome. Although these results are for fixed dielectric constant and conductivity, they represent typical integrand behavior throughout the range of interest.

The number of oscillations in the interval $\lambda \in [0, K_2]$ which are due to the exponential term $\exp(-(\lambda^2 - K_2^2)^{1/2}|z + z'|)$ is given by $|z + z'|$ divided by the free-space wavelength. As $|z + z'|$ becomes large in terms of free-space wavelengths, these oscillations become rapidly varying near the branch point at λ equal to K_2. Integration of these oscillations is further complicated by the peaked behavior of the integrand that occurs near this branch point. Figure 2 illustrates this behavior for the first two components of (7). Since the remaining components (equation (7)) behave similarly, attention will be focused on these first two components throughout this paper. In Figure 2, ρ equals 1 free-space wavelength, $z + z'$ equals 20 free-space wavelengths, the frequency f is 100 MHz, and the earth's relative dielectric constant and conductivity are 16 and 0.0001 mhos/m, respectively.

To make these densely packed oscillations more evenly spaced and to remove the peaked behavior of the integrand at branch point, the transformation

$$\lambda = K_2 \sin\theta \qquad \theta \in \left[0, \frac{\pi}{2}\right] \tag{8}$$

is employed over the λ interval $[0, K_2]$. The branch in the exponent

$$\exp[-(\lambda^2 - K_2^2)^{1/2}|z + z'|] = \exp[-iK_2|z + z'|\cos\theta] \tag{9}$$

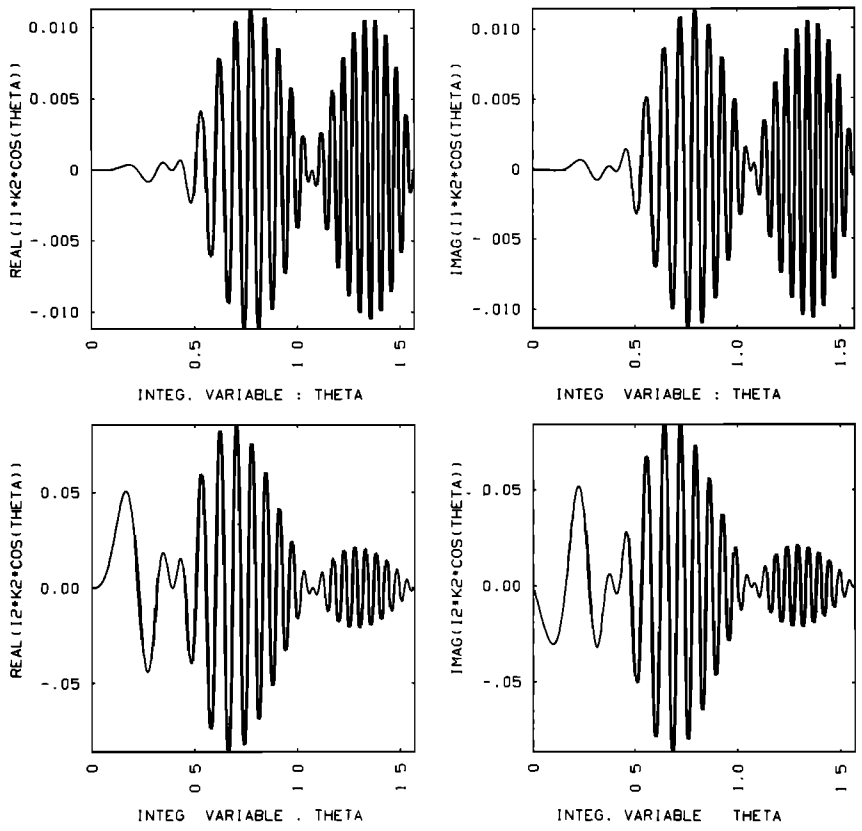

Fig. 3. Behavior of the transformed integrands in the θ interval $[0, \pi/2]$. Parameters: $f = 10^8$ Hz, $\varepsilon_r = 16$, $\sigma = 10^{-4}$ mhos/m, $\rho = 1\lambda_0$, and $z + z' = 20\lambda_0$.

is removed by this transformation. Since

$$d\lambda = K_2 \cos\theta \, d\theta \tag{10}$$

a typical denominator (equation (7)) multiplied by the transformation's Jacobian equals

$$D_1 = \frac{K_2 \cos\theta}{K_1^2\gamma_2 + K_2^2\gamma_1} = \frac{\cos\theta}{K_1^2 \cos\theta + K_2(K_2^2 \sin^2\theta - K_1^2)^{1/2}} \tag{11}$$

and remains nonsingular even when K_1 approaches K_2. The results of this transformation on the integrands I1 and I2 are shown in Figure 3. In contrast to Figure 2, the oscillations are more evenly spaced and the peaked behavior of the integrand no longer occurs.

A similar transformation may be used in the λ interval $[K_2, 2K_2]$. This transformation is given by

$$\lambda = K_2 \sec\theta \qquad \theta \in [0, \cos^{-1}(0.5)] \tag{12}$$

Again the branch in the exponent

$$\exp[-(\lambda^2 - K_2^2)^{1/2}|z + z'|] = \exp[-K_2|z + z'| \tan\theta] \tag{13}$$

is no longer present. Also,

$$d\lambda = K_2 \sec\theta \tan\theta \, d\theta \tag{14}$$

so that a typical denominator (equation (7)) multiplied by the transformation's Jacobian equals

$$D_2 = \frac{\sec\theta \tan\theta}{K_1^2 \tan\theta + K_2(K_2^2 \sec^2\theta - K_1^2)^{1/2}} \tag{15}$$

which is nonsingular even when K_1 equals K_2.

When $|z + z'|$ is large, the rapid decay of the exponential $\exp(-(\lambda^2 - K_2^2)^{1/2}|z + z'|)$ facilitates integration for $\lambda > K_2$. This is illustrated in Figure 4, which has the same parameters as Figures 2 and 3. In particular, $z + z'$ equals 20 wavelengths while ρ equals 1 wavelength. As discussed previously, the transformation in (12) aids integration in the λ inter-

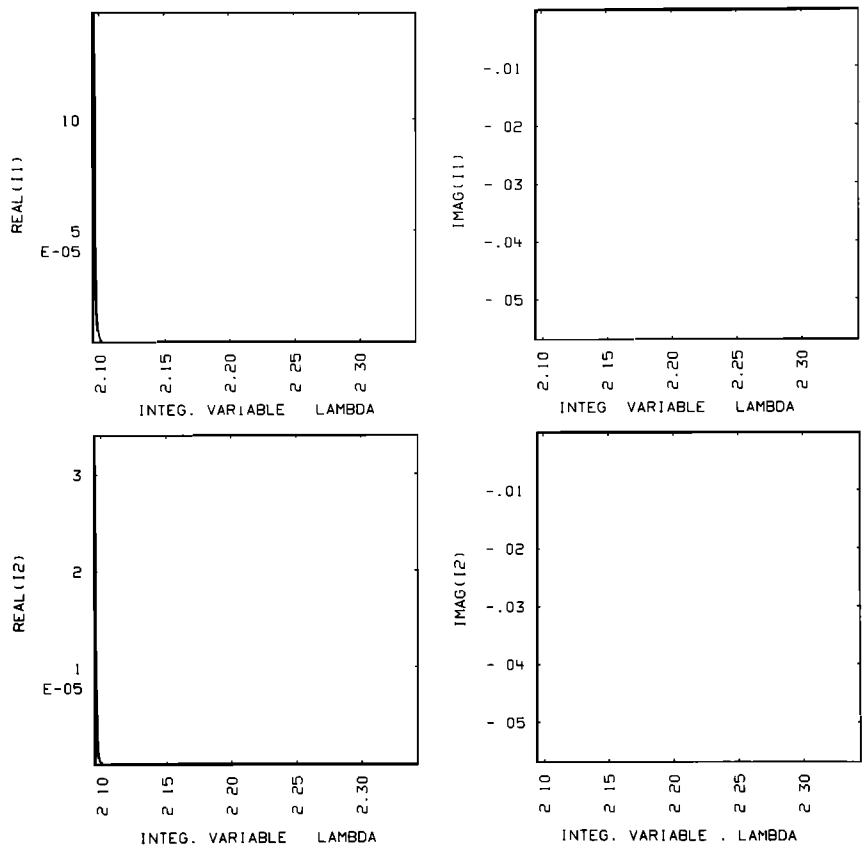

Fig. 4. Integrand behavior in the λ interval $[K_2, \infty]$. Parameters: $f = 10^8$ Hz, $\varepsilon_r = 16$, $\sigma = 10^{-4}$ mhos/m, $\rho = 1\lambda_0$, and $z + z' = 20\lambda_0$.

val $[K_2, 2K_2]$. In the interval $[2K_2, \infty)$, no transformation is necessary.

As $z + z'$ becomes small relative to ρ, integration over the interval $[2K_2, \infty)$ becomes difficult due to oscillations of the Bessel functions and slow exponential decay. Figure 5 shows the behavior of the integrands I1 and I2. In this figure, $z + z'$ and ρ have been set to 0.01 and 2 free-space wavelengths, respectively. All other parameters remain unchanged.

To accomplish the integration under these conditions, it is convenient to express (6) as

$$\int_0^\infty \bar{I}(\lambda, |z + z'|, \rho)\, d\lambda$$

$$= \int_0^\infty [\bar{I}(\lambda, |z + z'|, \rho) - \overline{\text{ASYM}}(\lambda, |z + z'|, \rho)]\, d\lambda$$

$$+ \int_0^\infty \overline{\text{ASYM}}(\lambda, |z + z'|, \rho)\, d\lambda \qquad (16)$$

where $\overline{\text{ASYM}}$ is the asymptotic approximation to $\bar{I}$ given by

$$\overline{\text{ASYM}}(\lambda, w, \rho) = \begin{bmatrix} \dfrac{e^{-\lambda w} J_0(\lambda\rho)}{K_2^2 + K_1^2}\left(\lambda^2 + \dfrac{K_2^2 w}{2}\lambda + \dfrac{K_2^4 w^2}{8} + \dfrac{K_1^2 K_2^2}{K_1^2 + K_2^2}\right) \\ \quad \cdot 5e^{-\lambda w} J_0(\lambda\rho) \\ \dfrac{e^{-\lambda w} J_1(\lambda\rho)}{K_2^2 + K_1^2}\left(\lambda^2 + \dfrac{K_2^2 w}{2}\lambda + \dfrac{K_2^4 w^2}{8} - \dfrac{K_2^2}{2} + \dfrac{K_1^2 K_2^2}{K_1^2 + K_2^2}\right) \\ \dfrac{e^{-\lambda w} J_1(\lambda\rho)}{K_2^2 + K_1^2}\left(\lambda + \dfrac{K_2^2 w}{2}\right) \end{bmatrix} \qquad (17)$$

These asymptotic forms have been derived in Appendix A. The second integral on the right of (16) has been obtained in closed form (Appendix A).

Figure 6 illustrates the behavior of the integrand when the asymptotic terms (Equation (17)) are subtracted from $\bar{I}$ (Equations (6) and (7)). The results are

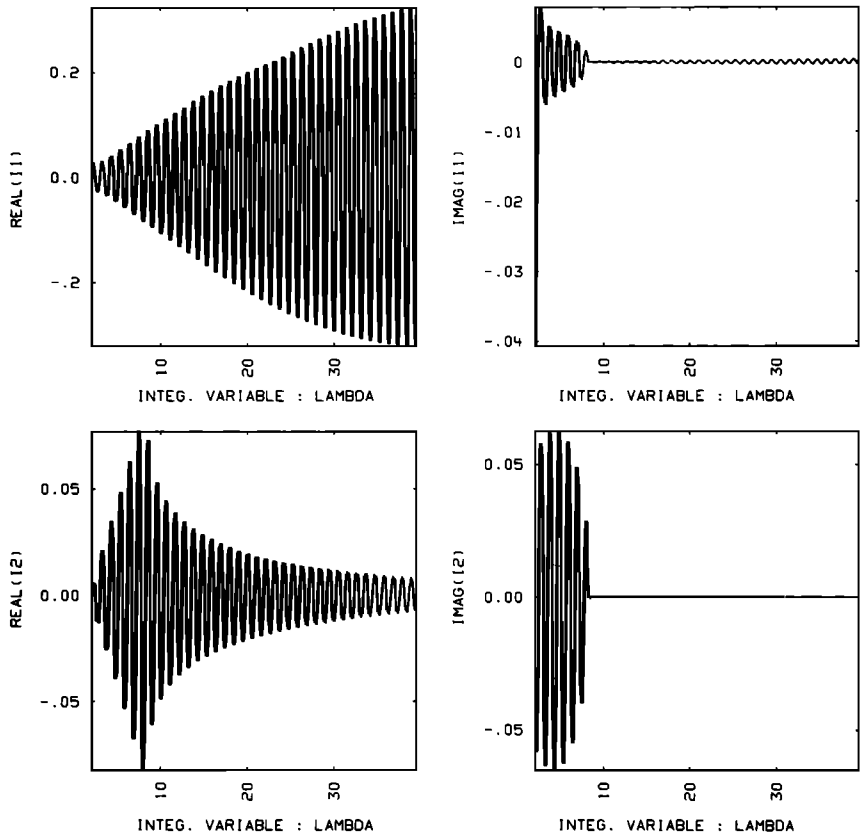

Fig. 5. Small exponential decay requires subtraction of asymptotic terms from the integrands in the λ interval $[K_2, \infty]$. Parameters: $f = 10^8$ Hz, $\varepsilon_r = 16$, $\sigma = 10^{-4}$, $\rho = 2\lambda_0$, and $z + z' = 0.01\lambda_0$.

shown for the first two components only, since the behavior of the remaining two components is similar. Clearly, these integrands are much more amenable to numerical integration than those of Figure 5 because of their faster rates of decay. The implementation of the analysis of this section by algorithmic means is left to Appendices B and C.

4. SAMPLE NUMERICAL RESULTS

In this section the real axis integration technique is compared with the complex contour methods of *Burke et al.* [1981]. Both programs were run on a CDC-7600 computer, and the computer run times were recorded. In each case both the Hankel and Bessel contours of *Burke et al.* [1981] were used. The better of these results were recorded. In Tables 1–4 the first two components of the integrals in (6) multiplied by the free-space wavelength λ_0 are recorded as (a, b), with a and b the real and imaginary parts of the result, respectively. Although brevity considerations allow only the first two components to be shown, computation times are given for the evaluation of all four components of (6).

In Tables 1–3 the frequency is 10^8 Hz, and the earth's relative dielectric constant and conductivity are 16 and 10^{-4} mhos/m, respectively. The number of points in the compound Simpson's rule (Appendix B) is 2^{IPTS}, where IPTS equals 3. The truncation criteria CONV (Appendix C) is 10^{-4}, 10^{-3}, and 10^{-4} for Tables 1, 2, and 3, respectively.

In Table 1, $z + z'$ is 10 free-space wavelengths, while ρ decreases from 5 to 0.1 free-space wavelengths. Subtraction of asymptotic terms was not needed for each real axis integration. For large ρ values, the complex Hankel contour is more efficient. However, as ρ decreases, the real axis integration becomes significantly more efficient. The Bessel contour has not been shown, since the Hankel results were faster. Similar results are shown in Table 2, where $z + z'$ is set to 3 free-space wavelengths and ρ varies from 3 to 0.01 free-space wavelengths. Again,

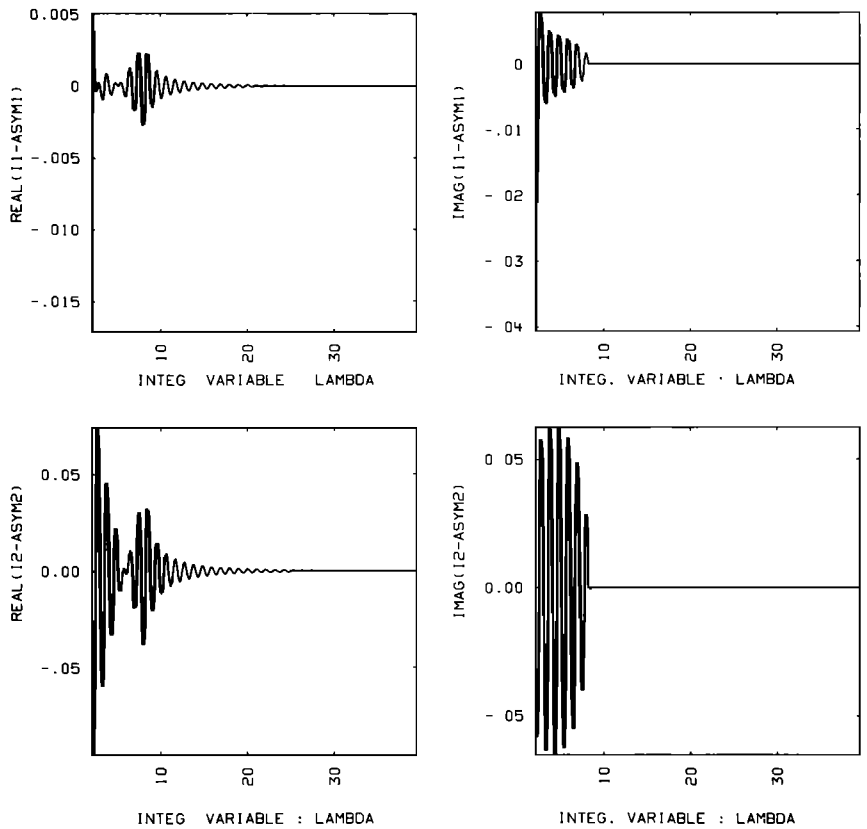

Fig. 6. Behavior of integrands for Figure 5 after asymptotic terms are subtracted. Parameters: $f = 10^8$ Hz, $\varepsilon_r = 16$, $\sigma = 10^{-4}$ mhos/m, $\rho = 2\lambda_0$, and $z + z' = 0.01\lambda_0$.

as ρ decreases, real axis integration becomes advantageous. In Table 3, ρ is set to 1 wavelength and $z + z'$ decreases from 1 wavelength to zero. Throughout, the real axis times are comparable to the Hankel contour, but computer experiments indicate the Hankel contour to be more accurate for $z + z'$ near zero and ρ equal to 1 free-space wavelength.

Table 4 shows sample calculations at a frequency of 2×10^6 Hz and earth's conductivity and relative dielectric constants of 0.01 mhos/m and 2, respec-

TABLE 1. A Comparison of Numerical Results as ρ Varies and $z + z' = 10\lambda_0$

	Distance in Wavelengths			
	$z + z' = 10\lambda_0$, $\rho = 5\lambda_0$	$z + z' = 10\lambda_0$, $\rho = 2.5\lambda_0$	$z + z' = 10\lambda_0$, $\rho = 1\lambda_0$	$z + z' = 10\lambda_0$, $\rho = 0.1\lambda_0$
Real axis	no asymptotics	no asymptotics	no asymptotics	no asymptotics
$\lambda_0((\partial^2/\partial z^2) + K_2^2)V_{22}$	(8.880E-4, −1.521E-3)	(4.615E-5, −6.308E-4	(1.951E-4, 2.625E-4)	(8.628E-6, 3.201E-4)
$\lambda_0 U_{22}$	(1.359E-2, −2.992E-2)	(1.387E-2, −3.531E-4)	(3.758E-2, −1.266E-2)	(3.999E-2, −5.870E-4)
CDC 7600 computer time, s	6.7E-2	5.8E-2	5.2E-2	4.2E-2
Complex contour	Hankel	Hankel	Hankel	Hankel
$\lambda_0((\partial^2/\partial z^2) + K_2^2)V_{22}$	(8.880E-4, −1.521E-3)	(4.612E-5, −6.306E-4)	(1.952E-4, 2.620E-4)	(8.625E-6, 3.183E-4)
$\lambda_0 U_{22}$	(1.359E-2, −2.992E-2)	(1.387E-2, −3.531E-2)	(3.759E-2, −1.266E-2)	(4.000E-2, −5.851E-4)
CDC 7600 computers time, s	4.8E-2	6.3E-2	8.7E-2	1.0E-1

Parameters: $f = 10^8$ Hz, $\sigma = 10^{-4}$ mhos/m, $\varepsilon_r = 16$, IPTS = 3, and CONV = 10^{-4}.

TABLE 2. A Comparison of Numerical Results as ρ Varies and $z + z' = 1\lambda_0$

	Distance in Wavelengths			
	$z + z' = 3\lambda_0, \rho = 3\lambda_0$	$z + z' = 3\lambda_0, \rho = 1\lambda_0$	$z + z' = 3\lambda_0, \rho = 0.1\lambda_0$	$z + z' = 3\lambda_0, \rho = 0.01\lambda_0$
Real axis	no asymptotics	no asymptotics	no asymptotics	no asymptotics
$\lambda_0((\partial^2/\partial z^2) + K_2^2)V_{22}$	(5.496-4, −1.097E-2)	(3.947E-3, −1.476E-3)	(3.251E-4, 3.529E-3)	(2.526E-4, 3.544E-3)
$\lambda_0 U_{22}$	(7.147E-4, −7.185E-2)	(5.969E-2, −1.062E-1)	(1.333E-1, −6.643E-3)	(1.335E-1, −5.266-3)
CDC 7600 time, s	3.5E-2	2.8E-2	2.5E-2	2.54E-2
Complex contour	Hankel	Hankel	Hankel	Bessel
$\lambda_0((\partial^2/\partial z^2) + K_2^2)V_{22}$	(5.495E-4, −1.097E-2)	(3.948E-3, −1.476E-3)	(3.270E-4, 3.526E-3)	(2.546E-4, 3.540E-3)
$\lambda_0 U_{22}$	(7.152E-4, −7.185E-2)	(5.968E-2, −1.061E-1)	(1.333E-1, −6.631E-3)	(1.335E-1, −5.254E-3)
CDC 7600 time, s	6.4E-2	1.0E-1	8.3E-2	9.4E-2

Parameters: $f = 10^8$ Hz, $\sigma = 10^{-4}$ mhos/m, $\varepsilon_r = 16$, IPTS = 3, and CONV = 10^{-3}.

tively. Results of the real axis integration seem to agree with the complex contours to 3 or 4 significant digits throughout. Again, for ρ small, the real axis integration has a distinct advantage.

5. CONCLUSIONS AND RECOMMENDATIONS FOR FUTURE WORK

The real axis integration technique presented in this paper is particularly well suited for the analysis of thin wires vertical to the air-earth interface. This analysis is not suitable for a long horizontal antenna with $z + z'$ equal to zero. To cover efficiently a wide range of spatial parameters, it is prudent to combine real axis and complex contour integration techniques. For example, if one desires to compute Sommerfeld integrals in the region $((z + z')^2 + \rho^2)^{1/2}$ less than or equal to 1 wavelength as done by *Burke et al.* [1981], it is efficient to use real axis techniques for $z + z' \geq \rho$ and complex contour techniques in the remaining region. Since the region in which the real axis integration is used does not require subtraction of asymptotic terms, the technique is valid for a wide range of frequencies and medium parameters.

Since extension of real axis integration of Sommerfeld integrands to the case where one or both of source and observer lies below the ground is straightforward, but tedious, results have not been given. It may be possible to extend results to lower frequencies by subtraction of higher order asymptotic terms. Use of integration routines other than Simpson's rule may be more efficient but would not change the basic conclusions of this paper. Horizontal rings of $\hat{\rho}$- and $\hat{z}$-directed current with aximuth symmetry may also be treated by this technique. The problem of a vertical cylinder which penetrates the air-earth interface and is excited by an aximuthally symmetric voltage source will be treated with these techniques in a future paper.

TABLE 3. A Comparison of Numerical Results With $z + z'$ Variable and ρ Fixed

	Distance in Wavelengths			
	$z + z' = 1\lambda_0, \rho = 1\lambda_0$	$z + z' = 0.1\lambda_0, \rho = 1\lambda_0$	$z + z' = 0.01\lambda_0, \rho = 1\lambda_0$	$z + z' = 0, \rho = 1\lambda_0$
Real axis	no asymptotics	with asymptotics	with asymptotics	with asymptotics
$\lambda_0((\partial^2/\partial z^2) + K_2^2)V_{22}$	(−2.898E-2, −1.809E-2)	(6.451E-2, −4.516E-2)	(6.047E-2, −4.724E-2)	(5.984E-2, −4.701E-2)
$\lambda_0 U_{22}$	(−1.976E-1, −9.064E-2)	(4.521E-2, −2.192E-2)	(3.560E-2, 4.369E-2)	(5.185E-4, 6.245E-2)
CDC 7600 computer time, s	3.0E-2	5.4E-2	1.1E-1	1.1E-1
Complex contour	Hankel	Hankel	Hankel	Hankel
$\lambda_0((\partial^2/\partial z^2) + K_2^2)V_{22}$	(−2.900E-2, −1.808E-2)	(6.452E-2, −4.516E-2)	(6.045E-2, −4.725E-2)	(5.980E-2, −4.701E-2)
$\lambda_0 U_{22}$	(−1.976E-1, −9.059E-2)	(4.526E-2, −2.195E-2)	(3.376E-3, 4.369E-2)	(−6.417E-5, 6.245E-2)
CDC 7600 computer time, s	6.7E-2	1.1E-2	1.E-1	1.1E-1

Parameters: $f = 10^8$ Hz, $\sigma = 10^{-4}$ mhos/m, $\varepsilon_r = 16$, IPTS = 3, and CONV = 10^{-4}.

TABLE 4. Typical Numerical Results at 2 Megahertz

	Distance in Wavelengths			
	$z + z' = 0, \rho = 0.5\lambda_0$	$z + z' = 0, \rho = 0.01$	$z + z' = 3\lambda_0, \rho = 3\lambda_0$	$z + z' = 3\lambda_0, \rho = 0.1\lambda_0$
Real axis	with asymptotics	with asymptotics	no asymptotics	no asymptotics
$\lambda_0((\partial^2/\partial z^2) + K_2^2)V_{22}$	(−2.557E-2, −3.798E-2)	(−1.835E-1, −5.611E-2)	(2.393E-3, −1.103E-4)	(−7.244E-4, 1.253E-4)
$\lambda_0 U_{22}$	(−1.420E-2, 4.568E-3)	(7.308E-1, −2.079E-1)	(2.241E-2, 2.472E-2)	(5.188E-2, 3.915E-2)
CDC 7600 time, s	1.6E-1	7.0E-2	3.5E-2	2.5E-2
Complex contour	Hankel	Hankel	Hankel	Bessel
$\lambda_0((\partial^2/\partial z^2) + K_2^2)V_{22}$	(−2.562E-2, −3.801E-2)	(−1.840E-1, −5.618E-2)	(2.393E-3, −1.103E-4)	(−7.240E-4, 1.256E-4)
$\lambda_0 U_{22}$	(−1.413E-2, 4.666E-3)	(7.309E-1, −2.0778E-1)	(2.240E-2, −2.472E-2)	(5.189E-2, 3.917E-2)
CDC 7600 time, s	9.E-2	1.2E-1	3.6E-2	9.1E-2

Parameters: $\sigma = 10^{-2}$ mhos/m, $\varepsilon_r = 2$, IPTS = 3, and CONV = 10^{-5}.

APPENDIX A: ASYMPTOTIC FORMS OF THE SOMMERFELD INTEGRANDS

To overcome difficulties associated with the slow exponential decay of the integrands (equation (6)) as $|z + z'|$ becomes small, section 3 has made use of their asymptotic forms. These asymptotic forms are now obtained along with closed form expressions for their integrals over the definite interval $\lambda \in [0, \infty)$.

To obtain the desired result, some preliminary groundwork is necessary. For large λ,

$$(\lambda^2 - K_i^2)^{1/2} \approx \lambda - \frac{K_i^2}{2\lambda} \qquad i = 1, 2 \tag{A1}$$

$$e^{-\lambda_2 w} \approx e^{-\gamma w}\left(1 + \frac{K_2^2 w}{2\lambda} + \frac{K_2^4 w^2}{8\lambda^2}\right) \tag{A2}$$

$$\frac{1}{K_2^2\gamma_1 + K_1^2\gamma_2} \approx \frac{1}{K_2^2 + K_1^2}\frac{1}{\lambda}\left(1 + \frac{K_2^2 K_1^2}{K_2^2 + K_1^2}\frac{1}{\lambda^2}\right) \tag{A3}$$

and

$$\frac{1}{\gamma_2 + \gamma_1} \approx \frac{1}{2\lambda}\left(1 + \frac{K_1^2 + K_2^2}{4\lambda^2}\right) \tag{A4}$$

From these expressions an asymptotic approximation, $\overline{\text{ASYM}}$, to $\bar{I}$ (equation (7)) may be obtained. The result is

$$\text{ASYM1} = \frac{e^{-\lambda w}J_0(\lambda\rho)}{K_1^2 + K_2^2}\left(\lambda^2 + \frac{K_2^2 w}{2}\lambda + \frac{K_2^4 w^2}{8} + \frac{K_1^2 K_2^2}{K_1^2 + K_2^2}\right) \tag{A5}$$

$$\text{ASYM2} = 0.5e^{-\lambda w}J_0(\lambda\rho) \tag{A6}$$

$$\text{ASYM3} = \frac{e^{-\lambda w}J_0(\lambda\rho)}{K_2^2 + K_1^2}\left(\lambda^2 + \frac{K_2^2 w}{2}\lambda + \frac{K_2^4 w^2}{8} - \frac{K_2^2}{2} + \frac{K_1^2 K_2^2}{K_1^2 + K_2^2}\right) \tag{A7}$$

and

$$\text{ASYM4} = \frac{e^{-\lambda w}}{K_2^2 + K_1^2}J_1(\lambda\rho)\left(\lambda + \frac{K_2^2 w}{2}\right) \tag{A8}$$

In the above asymptotic expressions, terms which decrease faster than $e^{-\lambda w}J_0(\lambda\rho)$ have not been included so that the expressions may be integrated from zero to infinity analytically.

To obtain a closed form expression for the integral

$$\bar{Z} = \int_0^\infty \overline{\text{ASYM}}(\lambda)\, d\lambda \tag{A9}$$

recall [*Abramowitz and Stegun*, 1970]

$$T0 = \int_0^\infty e^{-\lambda w}J_0(\lambda\rho)\, d\lambda = \frac{1}{(w^2 + \rho^2)^{1/2}} \tag{A10}$$

$$T1 = \int_0^\infty e^{-\lambda w}J_0(\lambda\rho)\, \lambda d\lambda = -\frac{\partial}{\partial w}\frac{1}{(w^2 + \rho^2)^{1/2}} = \frac{w}{(w^2 + \rho^2)^{3/2}} \tag{A11}$$

$$T2 = \int_{0ZS\infty} e^{-\lambda w}\lambda^2 J_0(\lambda\rho)\, d\lambda = \frac{\partial^2}{\partial w^2}\frac{1}{(w^2 + \rho^2)^{1/2}} = \frac{2w^2 - \rho^2}{(w^2 + \rho^2)^{5/2}} \tag{A12}$$

Similarly,

$$U0 = \int_0^\infty e^{-\lambda w}J_1(\lambda\rho)\, d\lambda = \frac{1}{\rho}\frac{(w^2 + \rho^2)^{1/2} - w}{(w^2 + \rho^2)^{1/2}} \tag{A13}$$

$$U1 = \int_0^\infty e^{-\lambda w}\lambda J_1(\lambda\rho)\, d\lambda = -\frac{\partial}{\partial\rho}\int_0^\infty e^{-\lambda w}J_0(\lambda\rho)\, d\lambda = \frac{\partial}{\partial\rho}\frac{1}{(\rho^2 + w^2)^{1/2}} = \frac{\rho}{(\rho^2 + w^2)^{3/2}} \tag{A14}$$

and

$$U2 = \int_0^\infty e^{-\lambda w}\lambda^2 J_1(\lambda\rho)\, d\lambda = \frac{\partial^2}{\partial w\, \partial\rho}\int_0^\infty e^{-\lambda w} J_0(\lambda\rho)\, d\lambda$$

$$= \frac{\partial^2}{\partial w\, \partial\rho}\frac{1}{(\rho^2 + w^2)^{1/2}} = \frac{3\rho w}{(\rho^2 + w^2)^{5/2}} \tag{A15}$$

From equations (A5)–(A15) it follows that

$$\bar{Z} = \begin{bmatrix} \dfrac{1}{K_2^2 + K_1^2}\left(T2 + \dfrac{K_2^2 w}{2}\, T1 + \dfrac{K_2^4 w^2}{8} + \dfrac{K_1^2 K_2^2}{K_1^2 + K_2^2}\, T0\right) \\ 0.5T0 \\ \dfrac{1}{K_2^2 + K_1^2}\left(U2 + \dfrac{K_2^2 w}{2}\, U1 + \dfrac{K_2^2 w}{8} - \dfrac{K_2^2}{2} + \dfrac{K_1^2 K_2^2}{K_1^2 + K_2^2}\, U0\right) \\ \dfrac{1}{K_2^2 + K_1^2}\left(U1 + \dfrac{K_2^2 w}{2}\, U0\right) \end{bmatrix} \tag{A16}$$

Thus a closed form expression for equation (A9) has been obtained.

APPENDIX B: NUMERICAL IMPLEMENTATION

The analysis in section 3 has been implemented by means of a FORTRAN computer program. A brief description of how the algorithm works is now given. Attention is first focused on the case where the exponential term $\exp(-(\lambda^2 - K_2^2)^{1/2}\,|z + z'|)$ decays rapidly enough so that subtraction of asymptotic terms is not necessary. Integration of (6) with respect to λ over the three intervals $[0, K_2]$, $[K_2, T]$, and $[T, \infty)$ is considered separately, where

$$T = \frac{K_2 + (\mathrm{Re}\,(K_1^2))^{1/2}}{2} \tag{B1}$$

Finally, subtraction of the asymptotic terms is briefly discussed.

Equation (8) is used to transform the λ integration over $[0, K_2]$ to an integration with respect to θ over the interval $[0, \pi/2]$. The peaks and nulls of the real and imaginary parts of the exponent (equation (9)) are given by

$$\theta_n = \cos^{-1}\left(\frac{n\pi}{2K_2\,|z + z'|}\right)$$

$$n = 0, 1, 2, \cdots, n_{\max} \tag{B2}$$

where

$$n_{\max} = \mathrm{int}\left(\frac{2K_2\,|z + z'|}{\pi}\right)$$

The symbol int (x) denotes the largest integer less than or equal to x. The first 60 zeros of both $J_0(u)$ and $J_1(u)$ are interlaced and stored in increasing order in an array Z_i $(i = 1, \cdots, 120)$. It follows from equations (8) and (6) that the θ values corresponding to these zeros are given by

$$\theta_i = \sin^{-1}\frac{Z_i}{K_2\rho}$$

$$i = 1, \cdots, i_{\max} \qquad Z_{i_{\max}} \le K_2\rho \tag{B3}$$

If $|K_1|/K_2 > 5$ the θ value

$$\theta = \cos^{-1}|4K_2/K_1| \tag{B4}$$

is added to track the variation of equation (11). All of these θ values are combined and stored in increasing order. Integration between successive θ values, $[\theta_i, \theta_{i+1}]$, is carried out by a compound Simpson's rule with 2^{IPTS} points [*Davis and Rabinowitz*, 1975]. IPTS is an as yet undetermined input parameter.

Equation (12) is used to transform the λ interval $[K_2, T]$ into the θ interval $[0, \cos^{-1}(K_2/T)]$. To track the rapidly decaying exponential when $z + z'$ is large, the λ interval is subdivided by the points

$$\lambda = K_2, K_2 + \Delta, K_2 + 2\Delta, \cdots, K_2 + n\Delta, T \tag{B5}$$

where

$$\Delta = \min\left(\frac{0.4\pi}{K_2\,|z + z'|}, K_2\right) \tag{B6}$$

These values are easily converted into their corresponding θ values through equation (12). Next, the θ values corresponding to the zeros of the Bessel functions are computed from (6) and (7) along with the values of the Bessel function zeros that have been stored in an array. Use of this array may be avoided by replacing the zeros of the Bessel functions by their asymptotic values. If $|K_1| > 5K_2$, the θ value

$$\theta_0 = \tan^{-1}(4K_2/|K_1|) \tag{B7}$$

is added to the other θ values to insure accurate tracking of (15). Again, all of the θ values are stored in an array of increasing order, and a compound Simpson's rule is used to integrate between the successive values.

Integration of (6) over the interval $[2K_2, \infty)$ is accomplished without use of any variable transfor-

mations. To ensure adequate tracking of the denominators of (7), this interval is broken into two subintervals [T, RTRK1S] and [RTRK1S, ∞), where

$$\text{RTRK1S} = (\text{Re}\,(K_1^2))^{1/2} \tag{B8}$$

The first subinterval is further subdivided by the points

$$\lambda_0 = 2K_2 \qquad \lambda_1 = \lambda_0 + \text{STEP}, \cdots,$$
$$\lambda_{n_0-1} = \lambda_{n_0-2} + \text{STEP} \qquad \lambda_{n_0} = \text{RTRK1S} \tag{B9}$$

where STEP is set equal to Δ (equation (B6)) until λ is greater than $10K_2$, and then STEP is doubled each successive step. The second subinterval is also subdivided

$$\lambda_{n_0} = \text{RTRK1S} \qquad \lambda_{n_0+1} = \lambda_{n_0} + \text{STEP}$$
$$\lambda_{n_0+2} = \lambda_{n_0+1} + \text{STEP}, \cdots \tag{B10}$$

where STEP has been defined previously.

The λ values associated with the zeros of the Bessel functions are computed from the stored values of the Bessel functions' zero crossings and equation (7). Again, all of these λ values are stored in an array, and a compound Simpson's rule with 2^{IPTS} points is used to integrate between successive values.

Techniques for implementing the analysis of section 3 have been presented under the assumption that subtraction of the asymptotic terms (equations (16) and (17)) were not necessary. The same techniques may be applied without change when these asymptotic terms are subtracted from the integrand. A further comment on the procedure for truncating the integration over the infinite interval is left to Appendix C.

APPENDIX C: TRUNCATION OF THE INFINITE INTEGRATION INTERVAL

In Appendix B, techniques were presented for implementing the analysis of section 3. A discussion of how integration over the infinite interval [$2K_2$, ∞) is truncated was left for this appendix. Consideration is first given to the case when subtraction of asymptotic terms is not necessary.

In the case of significant exponential decay, say $z + z' \geq 0.5\rho$, the following truncation criterion has been found to be useful. As in Appendix B, the interval [$2K_2$, ∞) is divided into subintervals. It is convenient to express this as

$$[2K_2, \infty) = \bigcup_{i=0}^{\infty} [\lambda_i, \lambda_{i+1}] \tag{C1}$$

Numerical integration is performed on each segment. After each segment is integrated, a check is made to determine whether

$$\frac{\left| \int_{[\lambda_m, \lambda_{m+1}]} \bar{I}(\lambda, |z + z'|, \rho)\, d\lambda \right|}{\left| \sum_{i=0}^{n} \int_{[\lambda_i, \lambda_{i+1}]} \bar{I}(\lambda, |z + z'|, \rho)\, d\lambda \right|} \leq \text{CONV} \tag{C2}$$

where CONV is a convergence criterion that may be set by the user. If (C2) is satisfied IND consecutive times, where IND is a user-specified input parameter, the integration is truncated.

If $z + z' < 0.05\rho$, it has been found useful to use

$$\frac{\left| \sum_{j=0}^{3} \int_{[\lambda_{n+j}, \lambda_{n+1+j}]} \bar{I}(\lambda, |z + z'|, \rho)\, d\lambda \right|}{\left| \sum_{i=0}^{n+3} \int_{[\lambda_i, \lambda_{i+1}]} \bar{I}(\lambda, |z + z'|, \rho)\, d\lambda \right|} < \text{CONV} \tag{C3}$$

as a convergence criteria. It is seen from (B10) that the partition points not associated with the zeros of the Bessel functions become more widely spaced as λ becomes large. Thus the partition points asymptotically become the zeros of the Bessel functions. Asymptotically for large λ, the nulls of J_0 become the peaks of J_1 and vice versa, and the nulls become uniformly spaced. Thus the sum of the intervals in the numerator of (C3) approaches the distance between the nulls of either $J_0(\lambda\rho)$ or $J_1(\lambda\rho)$. This sum tends to be much smaller than any of the individual elements due to the oscillation of the Bessel functions.

If subtraction of asymptotic terms is necessary, one merely replaces $\bar{I}$ by $\bar{I} - \overline{\text{ASYM}}$ in (C2) and (C3) to obtain the truncation criteria. Similar criteria are used in the interval [K_2, T].

Acknowledgments. This work was performed by the Lawrence Livermore National Laboratory under the auspices of the U.S. Department of Energy under contract W-7405-ENG-48 and was supported by CORADCOM of the U.S. Army. D. G. Dudley contributed to this work while a summer visitor at Lawrence Livermore National Laboratory. The authors wish to thank C. M. Butler, R. W. Ziolkowski, and G. J. Burke for valuable discussions throughout the course of this work. The contributions of the reviewers to the clarity of this work are gratefully acknowledged.

REFERENCES

Abramowitz, M., and I. A. Stegun (1970), *Handbook of Mathematical Functions*, p. 1024, Dover, New York.

Banos, A. (1966), *Dipole Radiation in the Presence of a Conducting Half-Space*, Pergamon, New York.

Bubenik, D. M. (1977), A practical method for the numerical

evaluation of Sommerfeld integrals, *IEEE Trans. Antennas Propag., AP 25*(6), 904-906.

Burke, G. J., E. K. Miller, J. N. Brittingham, D. L. Lager, R. J. Lytle, and J. T. Okada (1981), Computer modeling of antennas near the ground, *Electromagnetics, 1*, 29–44.

Davis, P. J., and P. Rabinowitz (1975), *Methods of Numerical Integration*, pp. 45–48, Academic, New York.

Parhami, P., Y. Rahmat-Samii, and R. Mittra (1980), An efficient approach for evaluating Sommerfeld integrals encountered in the problem of a current element radiating over a lossy ground, *IEEE Trans. Antennas Propag., AP 28*(1), 100–104.

Rahmat-Samii, Y., R. Mittra, and P. Parhami (1981), Evaluation of Sommerfeld integrals for lossy half-space problems, *Electromagnetics, 1*, 1–28.

Rana, I. E., and N. G. Alexopoulos (1981), Current distribution and input impedance of printed dipoles, *IEEE Trans. Antennas Propag., AP 29*(1), 99–105.

Siegel, M., and R. W. P. King (1970), Electromagnetic fields in a dissipative half-space: A numerical approach, *J. Appl. Phys., 41*(6), 2415–2423.